ANALYSIS OF OPPORTUNITIES FOR INTERCALIBRATION BETWEEN TWO SPACECRAFT*

***Carlos M. Roithmayr*[†]*, and Paul W. Speth*[‡]
NASA Langley Research Center, Hampton, Virginia 23681, U.S.A.

Abstract

There is currently a strong interest in obtaining highly accurate measurements of solar radiation reflected by Earth. For example, the Traceable Radiometry Underpinning Terrestrial- and Helio- Studies (TRUTHS) satellite mission has been under consideration in Europe for several years, and planning is now under way for the Climate Absolute Radiance and Refractivity Observatory (CLARREO) spacecraft in the United States. Such spacecraft will provide measurements whose high accuracy is traceable to SI standards; these measurements will be useful as a reference for calibrating similar instruments on board other spacecraft. Hence, analysis of opportunities for intercalibration between two spacecraft plays an important role in the planning of future missions.

In order for intercalibration to take place, the measurements obtained from two spacecraft must have similar viewing geometry and be taken within a few minutes of one another. Viewing geometry is characterized in terms of viewing zenith angle, solar zenith angle, and relative azimuth angle. Opportunities for intercalibration are greater in number and longer in duration if the sensor with high accuracy can be aimed at points on the surface of the Earth other than the nadir or sub-satellite point.

Analysis of intercalibration over long periods is rendered tractable by making several simplifying assumptions regarding orbital motions of the two spacecraft about Earth, as well as Earth's orbit about the Sun. The shape of the Earth is also considered. A geometric construction called a "tent" is introduced to facilitate analysis. It is helpful to think of an intercalibration opportunity as the passage of one spacecraft through a tent that has a fixed shape and moves with the spacecraft whose measurements are to be calibrated. Selection of points on Earth's surface as targets for measurement is discussed, as is aiming the boresight of a steerable instrument. Analysis results for a pair of spacecraft in low Earth orbits are provided.

[†]E-mail address: Carlos.M.Roithmayr@nasa.gov

[‡]E-mail address: Paul.W.Speth@nasa.gov

1 INTRODUCTION

An understanding of the Earth's climate and a means to predict its behavior requires, among other things, highly accurate measurements of solar irradiance reflected by the planet into space. The need to obtain such measurements using spacecraft is therefore widely recognized within the scientific community. One mission that has been under consideration for some time in Europe is referred to as Traceable Radiometry Underpinning Terrestrial- and Helio- Studies (TRUTHS), as discussed in Refs. [1]–[3]. In its 2007 Decadal Survey report (Ref. [4]), the U.S. National Research Council recommends the Climate Absolute Radiance and Refractivity Observatory (CLARREO) as one of four missions to be given highest priority. Planning is now under way (Ref. [5]) for CLARREO, which is to be implemented jointly by NASA and NOAA. One important purpose of missions such as these will be to obtain measurements that can be used in a process referred to as intercalibration. That is, measurements collected by a highly accurate instrument on one spacecraft will be used to calibrate an instrument aboard another spacecraft. In this chapter we provide some important mathematical relationships needed in studying the orbital conditions under which intercalibration can occur. In addition, aspects of intercalibration measurements are characterized in an example involving two spacecraft in low Earth orbits.

Throughout the discussion that follows, the satellite from which highly accurate measurements are obtained is referred to as the primary spacecraft. The secondary spacecraft is the one whose instrument is to be calibrated using measurements furnished by the primary spacecraft. Measurements from the two spacecraft must be taken a short time apart, with similar viewing geometry, in order for intercalibration to occur. Roughly speaking, the opportunity for intercalibration occurs above a point on Earth's surface where the ground tracks of the spacecraft intersect, provided they pass over the point within a few minutes of each other. Because measurements involve reflected solar radiation, illumination of Earth must also be considered.

Comparison of measurements of reflected solar radiation obtained by two spacecraft in different orbits is a firmly established practice; several such comparisons are reviewed in Ref. [6]. One example, presented in Ref. [7], involves a Clouds and Earth's Radiant Energy System (CERES) instrument aboard the Tropical Rainfall Measuring Mission, and the Scanner for Radiation Budget (ScaRaB) instrument on a Resurs spacecraft. The ScaRaB instrument scanned in a direction perpendicular to the Resurs groundtrack, and CERES was operated in the manner necessary to match viewing geometry. Somewhat more complicated instrument motion was employed in comparisons of two CERES instruments, one aboard the Terra satellite and the other mounted on the Aqua spacecraft. In that case, discussed in Ref. [8], the two scan planes were made parallel to each other, but were not perpendicular to the groundtrack of either spacecraft. In this chapter we examine the former situation, in which the instrument on the secondary spacecraft performs crosstrack scans.

Intercalibrating measurements of infrared radiation emitted by Earth is important in studying climate, and in two respects the constraints to be met are more relaxed than those associated with intercalibrating measurements of reflected solar radiation. Infrared radiation can be measured whether or not Earth is illuminated, and a greater elapsed time between measurements can be tolerated. In this work, however, we confine our attention to reflected solar radiation.

In designing the primary spacecraft for intercalibration, and planning its orbital operations, it is important to be able to characterize several aspects of the related measurements over long periods of time. Information of interest includes the frequency, duration, and geographic distribution of opportunities for intercalibration, as well as viewing geometry for the measurements. Moreover, if it is possible to aim the instrument of the primary spacecraft so as to minimize or eliminate differences in viewing geometry, it is beneficial to know the details of how this can be accomplished.

The material in the chapter is organized as follows. Section 2 contains a presentation of simplifying assumptions regarding orbital motion of the spacecraft, planetary motion, and Earth's shape. Two geometrical constructions introduced in Sec. 3 facilitate the study of intercalibration opportunities; they are referred to as a "tent" and a "pyramid." Section 3 also contains a discussion of solar illumination. A treatment of intercalibration measurements is provided in Sec. 4 where viewing geometry is described in terms of three viewing angles, selection of a target point where viewing angles to the two spacecraft are identical is discussed, and rotation angles needed to aim an instrument boresight at the target are presented. A one-year example involving one spacecraft in a polar orbit and another in a sun-synchronous orbit is the focus of Sec. 5. Finally, concluding remarks are made in Sec. 6.

2 SIMPLIFYING ASSUMPTIONS

Orbital motion, more than anything else, is what determines the times and positions at which measurements taken by two spacecraft can be intercalibrated. Other important factors include the orbital motion of Earth about the Sun, the orientation of Earth in an inertial reference frame, and the position of a point on Earth's surface that serves as a target for the measurement taken by each spacecraft. Positions of such points are in turn determined by the planet's shape. Analysis of intercalibration is rendered tractable by making several simplifying assumptions regarding orbital motion, as well as planetary motion and shape.

2.1 Spherical Surface of Earth

The shape of the Earth is more closely approximated by an oblate spheroid than by a sphere. The equatorial radius is approximately 20 km greater than the polar radius. This difference is ignored and Earth's surface is regarded as a sphere of radius R_E, the equatorial radius, when calculating the latitude of a point on the surface, the altitude of a spacecraft above the surface, and the viewing angles introduced in Sec. 4.1. These quantities are therefore characterized as geocentric. Of course, accuracy can be improved by modeling Earth's surface as an oblate spheroid, and by calculating the geodetic counterparts to these quantities.

Earth's oblateness causes gravitational perturbations to a spacecraft's orbit that cannot be ignored, as discussed presently in Sec. 2.3.

2.2 Circular Orbits of Earth and Spacecraft

The orbit of a spacecraft about the Earth, as well as that of the Earth about the Sun, are assumed to be circular. The constant radius of the primary spacecraft's orbit is denoted

by R_C; likewise, the radius of the secondary spacecraft's orbit is indicated by R_A. The constant radius of Earth's orbit about the Sun is denoted by R_S.

An orbital parameter referred to as the argument of latitude, u, is the angle in the plane of the orbit between the ascending node and the position vector of a spacecraft. The argument of latitude changes with the time t according to the relationship

$$u = nt + u_0 \tag{1}$$

where u_0 is the value of u at time t_0, and where n is known as the mean motion. Mean motions for the primary spacecraft, secondary spacecraft, and Earth, are given by

$$n_C = \sqrt{\frac{\mu_E}{{R_C}^3}}, \qquad n_A = \sqrt{\frac{\mu_E}{{R_A}^3}}, \qquad n_S = \sqrt{\frac{\mu_S}{{R_S}^3}} \tag{2}$$

where the gravitational parameters of the Earth and Sun have, respectively, numerical values $\mu_E = 398600.436$ km^3/s^2 and $\mu_S = 1.327124399355 \times 10^{11}$ km^3/s^2. With $R_S = 1.4959787066 \times 10^8$ km, the value of n_S is determined to be 1.990984×10^{-07} rad/sec (0.9856 deg/day). In the case of Earth's heliocentric orbit u denotes an angle referred to as true longitude rather than argument of latitude. The plane of Earth's orbit, known as the ecliptic plane, is the fundamental plane used in measuring the inclination of all heliocentric orbits; therefore, the inclination of Earth's heliocentric orbit is zero, an ascending node does not exist, and argument of latitude is undefined.

By assuming Earth's orbit is circular, one is ignoring a slight eccentricity ($e = 0.0167$), and associated changes in angular speed and the distance from Earth to the Sun. Likewise, spacecraft orbits can in fact become non-circular because of aerodynamic drag and gravitational perturbations due to the Sun, the moon, and Earth's non-uniform mass distribution. Such perturbations, however, are typically dealt with through periodic maintenance of the orbit using a spacecraft's propulsion system.

2.3 One Orbital Perturbation: Earth Oblateness

In general, the oblateness of Earth has a pronounced effect over long periods of time on a spacecraft's orbit, which is completely described by six orbital elements. A common choice of orbital elements consists of a, semi-major axis distance; e, eccentricity; i, inclination of the orbit plane; Ω, longitude of the ascending node; ω, argument of periapsis; and u, argument of latitude. Oblateness produces an instantaneous time rate of change in all six orbital elements; however, when averaged over one orbit, the rates of change vanish for a, e, i, and u. For a circular orbit of radius R, the average rate of change in Ω is given by (see, for example, Ref. [9])

$$\left(\frac{d\Omega}{dt}\right)_{\text{av}} = -\frac{3}{2} n J_2 \left(\frac{R_E}{R}\right)^2 \cos i \tag{3}$$

where $J_2 = 1.08263 \times 10^{-3}$ is the zonal gravitational harmonic coefficient of degree 2 that quantifies oblateness. When R and i are chosen such that $(\dot{\Omega})_{\text{av}} = n_S$ [see Eqs. (2)], the orbit is sun-synchronous. The longitude of ascending node changes with the time t according to the relationship

$$\Omega = (\dot{\Omega})_{\text{av}}\, t + \Omega_0 \tag{4}$$

where Ω_0 is the value of Ω at time t_0.

In a circular orbit the periapsis is undefined, therefore we do not concern ourselves with the average time rate of change in ω.

2.4 Autumnal Equinox as Initial Epoch

The line of equinoxes is the line of intersection of Earth's equatorial plane and the ecliptic plane. The relative inclination of the two planes, known as the obliquity of the ecliptic, is approximately 23.44°. At some instant on the first day of Spring in the northern hemisphere, the position vector from Earth's center to the Sun's center is parallel to the line of equinoxes, and the direction of this vector is defined to be the vernal equinox direction. On the date of the autumnal equinox, the direction of the position vector from the Sun's center to Earth's center is the same as the vernal equinox direction. The time t_0 is defined to be the instant of the autumnal equinox.

It is assumed that the Earth spins about its polar axis at a constant angular speed and, further, at t_0 the spin angle is such that the line of equinoxes lies in the plane containing the Greenwich meridian. To be precise, the Greenwich meridian is facing away from the Sun.

For future work it may be desirable to have t_0 correspond to a particular year, month, day, hour, minute, and second, and to use the actual position and spin angle of Earth at that instant, as specified in Ref. [10] or another authoritative ephemeris.

3 INTERCALIBRATION OPPORTUNITY

An intercalibration opportunity is defined to be an interval of time during which it is possible for the primary spacecraft to obtain measurements that can be compared with those taken by the secondary spacecraft. If the instrument on the secondary spacecraft scans in the crosstrack direction (perpendicular to the spacecraft's ground track), it can be helpful to think of an opportunity in terms of the passage of the primary spacecraft through a "tent," a geometric construction that has a fixed shape and moves with the secondary spacecraft whose measurements are to be calibrated. When the primary spacecraft is inside the tent, intercalibration can take place. A geometric description of the tent is provided in Secs. 3.1 and 3.2. Another geometric construction, a pyramid that has four points in common with the tent, proves to be especially useful for determining the times at which an opportunity begins and ends, and the position of the primary spacecraft at each of those times, as discussed in Sec. 3.3. Because reflected solar radiation is being measured, solar illumination must also be considered in determining whether or not an opportunity in fact exists. Accordingly, solar illumination is the topic of Sec. 3.4.

3.1 Temporal Constraint

Reflected solar radiation lies in the shortwave region of the spectrum and the scenes observed by the instrument change rapidly; consequently, a limit is imposed on the time elapsed between a measurement obtained with the primary spacecraft and a measurement made from the secondary spacecraft, A (Ref. [11]). The time difference that can be tolerated depends on the purpose of the measurement comparison. In order to convey the idea

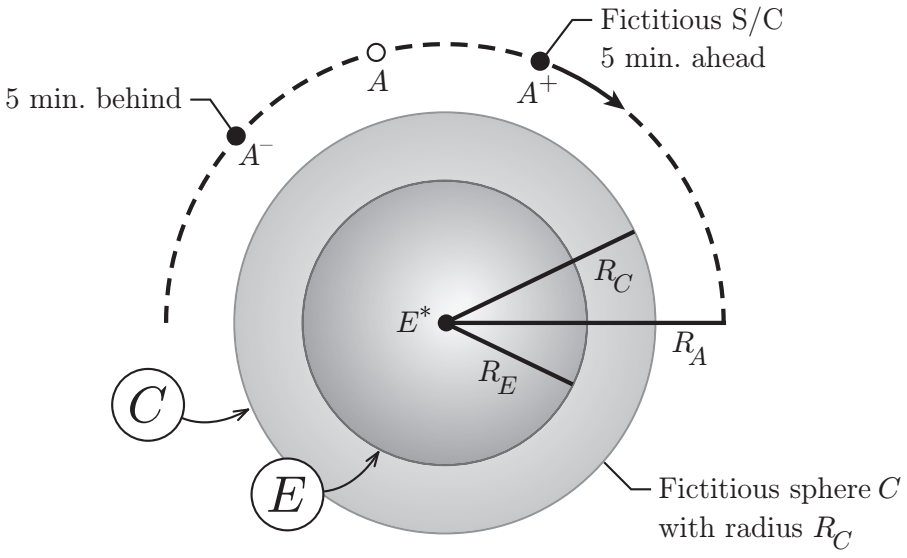

Figure 1. Fictitious Spacecraft, A^+ and A^-, with Temporal Displacements

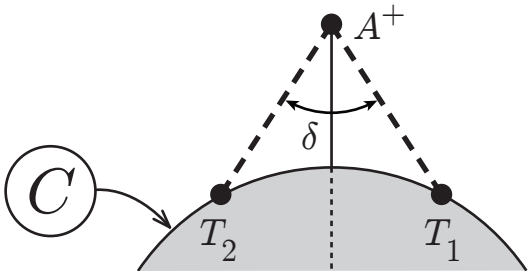

Figure 2. Leading Fictitious Spacecraft

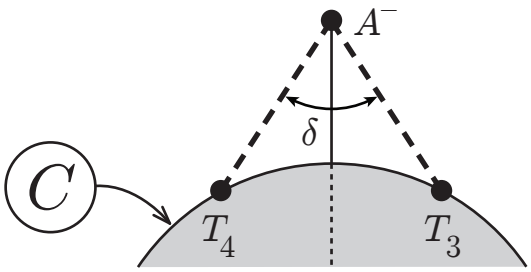

Figure 3. Trailing Fictitious Spacecraft

we employ a specific value and assume in what follows that the measurement by the primary spacecraft cannot be taken more than 5 minutes earlier than that of A, nor more than 5 minutes later. The determination of when and where this temporal constraint can be met is facilitated by the introduction of two fictitious spacecraft. The first such spacecraft, A^+, is 5 minutes ahead of A in the orbit, whereas the second such spacecraft, A^-, trails A by 5 minutes. This situation is illustrated in Fig. 1 for the case in which the radius R_A of the orbit of A is larger than the radius R_C of the the primary spacecraft's orbit. These spacecraft orbit the Earth, E, whose center is the point $E^\star$. At any instant of time, the position of the primary spacecraft lies somewhere on the surface of a fictitious sphere C. The curve between A^- and A^+ can be regarded as the ridge of a "tent."

3.2 Scan Angle of Instrument on Secondary Spacecraft

The boresight of the instrument aboard A is regarded as permanently aimed in the direction of local nadir (toward $E^\star$). The slope of the sides of the tent roof is determined by the angle δ, which is twice the scan angle of the instrument, as shown in Figs. 2 and 3. First, consider the spacecraft A^+ in Fig. 2. The field of view of the instrument is considered to lie in a plane that is perpendicular to the orbit plane of A; the curve between points T_1 and T_2 marks the intersection of the field of view and the surface of C. The plane containing A^+, T_1, and T_2 is regarded as the front face of the tent. Similarly, the rear face of the tent is the plane containing A^-, T_3, and T_4, as shown in Fig. 3.

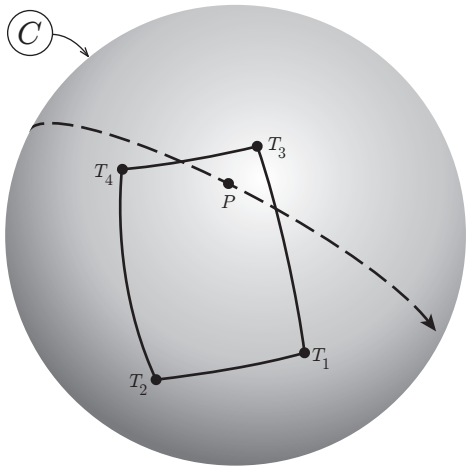

Figure 4. Upper Floor of the Tent

The four points T_1, T_2, T_4, and T_3 serve in pairs as the endpoints of four curves, each of which forms a boundary of a patch on the surface of C as indicated in Fig. 4. When the primary spacecraft, denoted by P, is inside the patch it is also inside the tent. An example of a path taken by P is illustrated in Fig. 4 with a dashed curve; in this case P enters through the rear face of the tent and exits through one side of the tent.

3.3 Intercalibration Pyramid

A determination of whether or not an intercalibration opportunity exists can be made with the aid of a right pyramid whose apex is $E^\star$ and whose base contains the points T_r ($r = 1, 2, 3, 4$), as depicted in Fig. 5. The position vector from $E^\star$ to A passes through the center of the pyramid's base and is fixed in the pyramid; therefore, the pyramid moves with A as it orbits E. The reader may recall that any rigid body can be regarded as a reference frame, and vice-versa. Thus, the pyramid can be considered as a local-vertical local-horizontal reference frame associated with the orbit of A.

Presently we will have occasion to make use of three right-handed mutually perpendicular unit vectors $\hat{\mathbf{a}}_1$, $\hat{\mathbf{a}}_2$, and $\hat{\mathbf{a}}_3$ fixed in the pyramid, as shown in Figs. 6 and 7. Unit vector $\hat{\mathbf{a}}_3$ is parallel to local vertical at A, and directed towards nadir. Unit vector $\hat{\mathbf{a}}_1$ lies in the orbit plane of A, and is in the direction of the orbital (circular) velocity of A. Finally, $\hat{\mathbf{a}}_2$ is perpendicular to the orbit plane of A and has direction opposite to $\mathbf{h}_A$, the orbital angular momentum vector of A.

Two constant angles are used to define the shape of the pyramid. The first of these is ψ, shown in a lateral cross section of the pyramid in Fig. 6. If the time interval allowed between measurements is denoted by τ (for example, $\tau = 5$ min $= 300$ sec), then ψ is simply the product of n_A [see Eqs. (2)] and τ,

$$\psi = n_A \, \tau \tag{5}$$

The second angle, ϵ, shown in a transverse cross section of the pyramid in Fig. 7, is calculated as follows. Consider a triangle having a base of length R_A (the distance from $E^\star$ to A), and three angles ϵ, $\delta/2$, and a (not shown). According to the law of sines for a plane triangle,

$$\frac{R_A}{\sin a} = \frac{R_C}{\sin(\delta/2)} \tag{6}$$

Because $\sin a = \sin(\pi - a)$, this relationship in general admits two solutions for a; one with $a < \pi/2$ and the other with $a > \pi/2$. The values of R_A, R_C, and δ encountered in studies to date correspond to the latter solution; however, the former solution is obtained numerically when using the function $\arcsin(\,)$. The difficulty is circumvented by calculating ϵ as

$$\epsilon = \pi - \delta/2 - (\pi - a) = a - \delta/2 \tag{7}$$

The result in Eq. (7) is used when $R_A > R_C$. On the other hand, when $R_A < R_C$, a revision of Figs. 1 – 3 and 5 – 7 must be undertaken, and the analysis leading to an expression for ϵ must be modified. The result in that case is $\epsilon = \delta/2 - a$.

With numerical values for ψ and ϵ in hand, one can perform two straightforward calculations involving $\mathbf{p}^{PE^\star}$, the position vector from P to $E^\star$. P is inside the tent when the following two inequalities are satisfied.

$$\left| \arctan\left(\frac{\mathbf{p}^{PE^\star} \cdot \hat{\mathbf{a}}_1}{\mathbf{p}^{PE^\star} \cdot \hat{\mathbf{a}}_3} \right) \right| \leq \psi, \qquad \left| \arctan\left(\frac{\mathbf{p}^{PE^\star} \cdot \hat{\mathbf{a}}_2}{\mathbf{p}^{PE^\star} \cdot \hat{\mathbf{a}}_3} \right) \right| \leq \epsilon \tag{8}$$

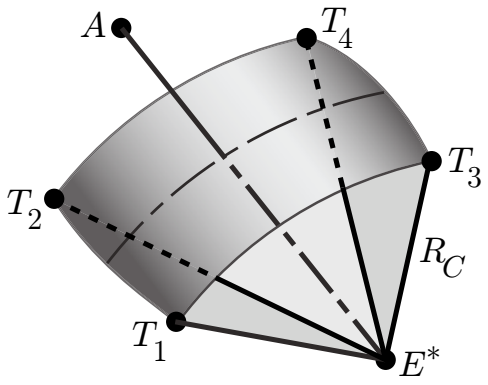

Figure 5. Intercalibration Pyramid

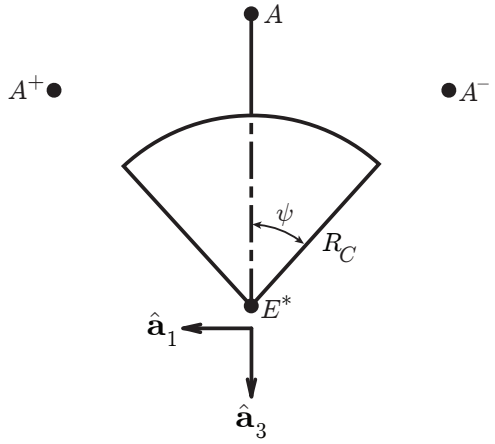

Figure 6. Lateral Cross Section of Pyramid

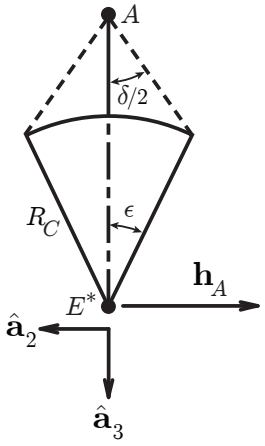

Figure 7. Transverse Cross Section of Pyramid

3.4 Solar Illumination

The discussion in Sec. 3.3 of the possibility of intercalibration fails to consider whether or not the measurements are taking place in sunlight. Solar illumination of the surface of E must be taken into account when dealing with measurements of reflected solar radiation.

In Fig. 8 the left hemisphere of E is in darkness whereas the right hemisphere of E is illuminated by the Sun. The circular boundary on the surface of E that separates the two hemispheres is known as the terminator. Spacecraft A is shown in a position directly above the terminator. In determining whether or not intercalibration of measurements of reflected solar radiation can be performed, it may be reasonable to require that P and A both be positioned somewhere over the illuminated hemisphere. The two requirements can be expressed mathematically as

$$\arccos(\mathbf{r}^{E^\star A} \cdot \mathbf{r}^{E^\star S}) \leq \pi/2, \qquad \arccos(\mathbf{r}^{E^\star P} \cdot \mathbf{r}^{E^\star S}) \leq \pi/2 \tag{9}$$

where $\mathbf{r}^{E^\star A}$, $\mathbf{r}^{E^\star P}$, and $\mathbf{r}^{E^\star S}$ are unit vectors having the same directions as the position vectors from $E^\star$ to A, P, and S (the Sun), respectively.

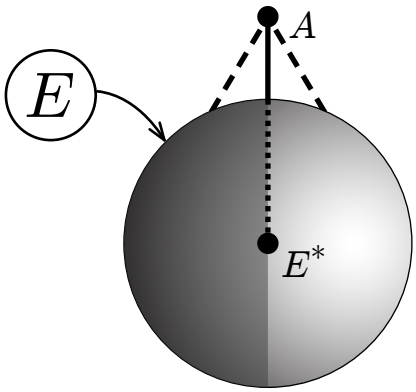

Figure 8. Illuminated Hemisphere

4 INTERCALIBRATION MEASUREMENTS

The general conditions necessary for intercalibration opportunities are presented in Sec. 3. During a single opportunity, several intercalibration measurements can be made. In order for such a measurement to be useful, a target on Earth's surface observed by spacecraft A must be viewed from a similar vantage point by spacecraft P. The viewpoint of each spacecraft is described in terms of three viewing angles introduced in Sec. 4.1. Selection of an instantaneous target point for a measurement taken by P is the subject of Sec. 4.2, and determination of the gimbal angles needed to aim the boresight of the instrument at this target is the focus of Sec. 4.3.

4.1 Viewing Angles

A measurement obtained by a spacecraft is associated with a specific point fixed on the surface of E. At any such target point, lines of sight to a spacecraft and to the Sun can

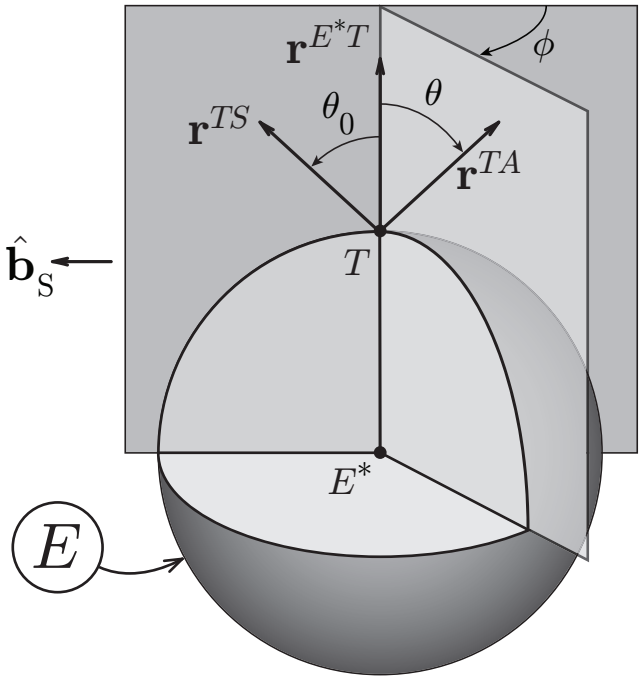

Figure 9. Viewing Angles

be described in terms of three angles. The three angles associated with a measurement taken from one spacecraft must have values that are similar to those corresponding to a measurement taken from another spacecraft in order for intercalibration to take place. An illustration of the three viewing angles is provided in Fig. 9.

At a target point T fixed to the surface of E, the viewing zenith angle θ is measured between a line that is locally vertical (zenith), and the line of sight to a spacecraft. A vector $\mathbf{r}^{E^\star T}$ with unit magnitude and the same direction as the position vector from $E^\star$ to T is parallel to zenith. A vector $\mathbf{r}^{TA}$ with unit magnitude and the same direction as the position vector from T to spacecraft A is parallel to the line of sight from T to A. Therefore,

$$\mathbf{r}^{E^\star T} \cdot \mathbf{r}^{TA} = \cos\theta \tag{10}$$

Provided $\theta \neq 0$, a unit vector normal to the plane containing $E^\star$, T, and A can be formed as

$$\hat{\mathbf{n}}_A = \frac{\mathbf{r}^{TA} \times \mathbf{r}^{E^\star T}}{|\mathbf{r}^{TA} \times \mathbf{r}^{E^\star T}|} \tag{11}$$

At T, the solar zenith angle θ_0 is measured between the zenith line and the line of sight to the Sun, S. Let $\mathbf{r}^{TS}$ be a unit vector having the same direction as the position vector from T to S. Thus,

$$\mathbf{r}^{E^\star T} \cdot \mathbf{r}^{TS} = \cos\theta_0 \tag{12}$$

Only when $\theta_0 \leq 75^\circ$ is a measurement of reflected solar radiation considered of value for the purpose of intercalibration (Ref. [12]). As long as $\theta_0 \neq 0$, a unit vector normal to the

plane containing $E^\star$, T, and S can be formed as

$$\hat{\mathbf{n}}_S = \frac{\mathbf{r}^{E^\star T} \times \mathbf{r}^{TS}}{|\mathbf{r}^{E^\star T} \times \mathbf{r}^{TS}|} \tag{13}$$

Subsequently a unit vector $\hat{\mathbf{b}}_S$, whose direction is called the solar backscatter direction, can be constructed as

$$\hat{\mathbf{b}}_S \triangleq \hat{\mathbf{n}}_S \times \mathbf{r}^{E^\star T} \tag{14}$$

Provided that neither θ or θ_0 vanishes, one can determine the angle ϕ between two planes; one contains $E^\star$, T, and S, and the other is formed by $E^\star$, T, and A. This angle, referred to as the relative azimuth angle, is related to the previously constructed unit vectors as follows.

$$\tan\phi = \frac{\hat{\mathbf{n}}_A \cdot \hat{\mathbf{b}}_S}{\hat{\mathbf{n}}_A \cdot \hat{\mathbf{n}}_S} \tag{15}$$

4.2 Boresight Target Point

The concept of an intercalibration tent is introduced in Sec. 3.1, and Fig. 4 depicts the upper floor of the tent as a patch on the surface of the sphere C. A similar patch on the surface of E can be regarded as the lower floor of the tent. Points on the lower tent floor are candidate targets for measurements that will meet the constraints imposed on time, illumination, and viewing angles discussed respectively in Secs. 3.3, 3.4, and 4.1. A particular target at which to aim the boresight of the instrument aboard P is determined with an approach[1] that will now be presented; at this target the viewing angles to P are, by construction, identical to those associated with Q, a particular one of an infinite number of (fictitious) spacecraft occupying the arc of radius R_A containing A^+, A, and A^-. As illustrated in Figs. 10 and 11, Q is the point on the arc between A^+ and A^- that is closest to P.

The position vector $\mathbf{p}^{E^\star P}$ from $E^\star$ to P can be regarded as the sum of two components; one lies in the orbit plane of A, whereas the other is perpendicular to the orbit plane of A. Let $\mathbf{q}$ be the first of these components and, henceforth, assume that P is inside the tent. One way of expressing $\mathbf{q}$ is

$$\mathbf{q} \triangleq (\mathbf{p}^{E^\star P} \cdot \hat{\mathbf{a}}_1)\hat{\mathbf{a}}_1 + (\mathbf{p}^{E^\star P} \cdot \hat{\mathbf{a}}_3)\hat{\mathbf{a}}_3 \tag{16}$$

where unit vectors $\hat{\mathbf{a}}_1$ and $\hat{\mathbf{a}}_3$ lie in the orbit plane of A and are directed as shown in Fig. 10. With $\mathbf{q}$ in hand, one may form the position vector from $E^\star$ to Q as

$$\mathbf{p}^{E^\star Q} \triangleq R_A \frac{\mathbf{q}}{|\mathbf{q}|} \tag{17}$$

The position vector from Q to P is given by

$$\mathbf{p}^{QP} = \mathbf{p}^{E^\star P} - \mathbf{p}^{E^\star Q} \tag{18}$$

When a line segment from Q to P is extended until it intersects E, the point of intersection T serves as a measurement target at which the viewing angles for P are, by construction,

[1] This method of choosing a target point was conceived by Donald P. Garber and David G. Macdonnell.

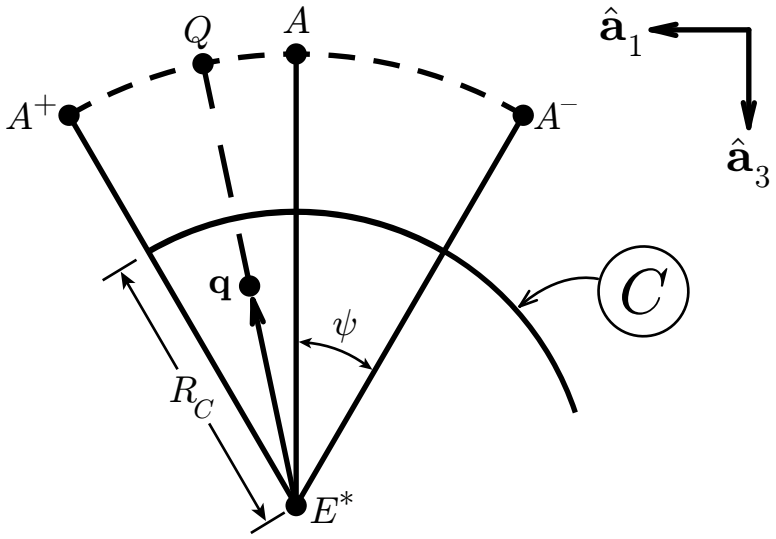

Figure 10. Projection of Position Vector to P (In-Plane View)

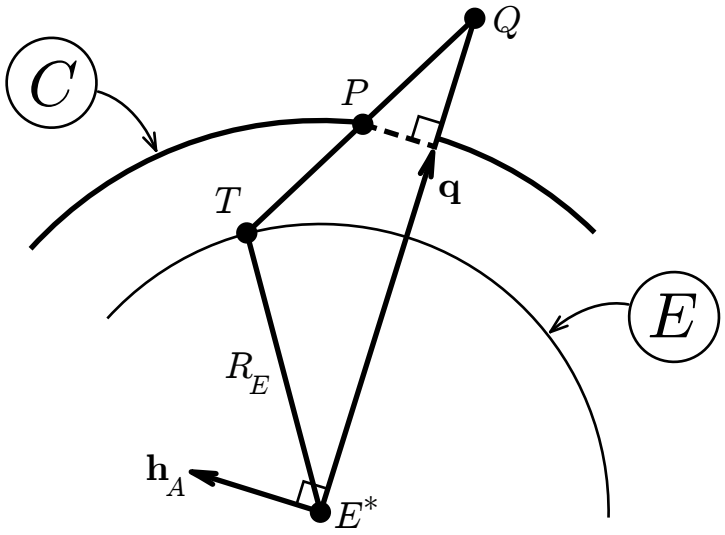

Figure 11. Projection of Position Vector to P (Out-of-Plane View)

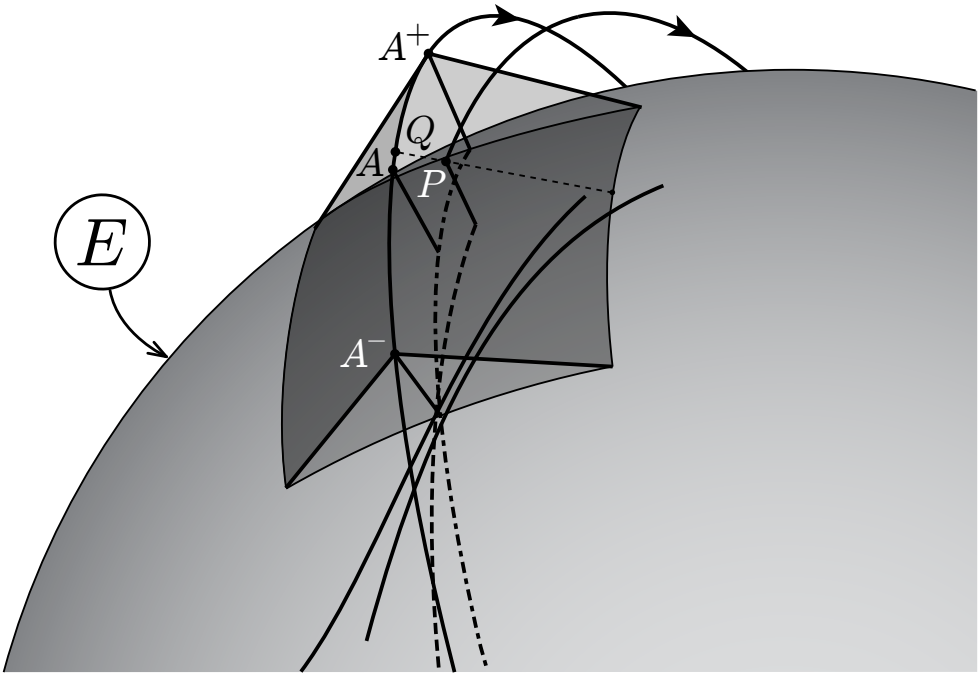

Figure 12. P Exits the Tent

identical to those for Q. The position vector $\mathbf{p}^{QT}$ from Q to T has the same direction as $\mathbf{p}^{QP}$, and a magnitude that can be determined on the basis of geometrical considerations. The position vector from $E^\star$ to T is then simply

$$\mathbf{p}^{E^\star T} = \mathbf{p}^{E^\star Q} + \mathbf{p}^{QT} \tag{19}$$

Figure 12 provides one example of a three-dimensional view of the locations of the aforementioned points of interest at the instant P exits the tent through the right side of the roof. The solid curved tracks shown on the surface of E mark the boundaries of the instrument's measurement swath as P passes through the tent.

4.3 Gimbal Angles

The reflected solar radiation instrument aboard P can be attached to the spacecraft bus by means of two revolute joints so that the instrument boresight can be aimed in various directions relative to the bus. The following material contains a discussion of how to determine the angular displacements in the joints or gimbals needed to aim the boresight at the target point identified in Sec. 4.2.

Figure 13 depicts a set of three right-handed, mutually perpendicular unit vectors $\hat{\mathbf{b}}_1$, $\hat{\mathbf{b}}_2$, and $\hat{\mathbf{b}}_3$ fixed in the spacecraft bus B such that they are parallel to the spacecraft roll, pitch, and yaw axes respectively. A similar set of unit vectors $\hat{\mathbf{d}}_1$, $\hat{\mathbf{d}}_2$, and $\hat{\mathbf{d}}_3$ is fixed in D, a rigid body in which the instrument is also fixed, with the boresight having the direction of $\hat{\mathbf{d}}_3$.

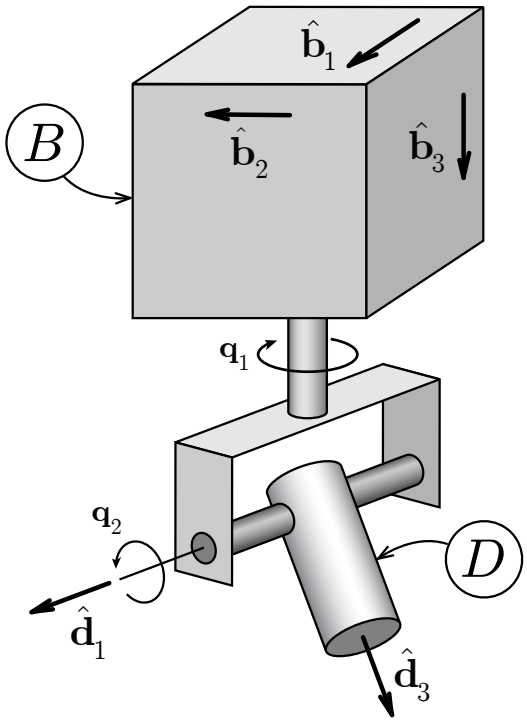

Figure 13. Primary Spacecraft with Gimbaled Instrument

The orientation of D with respect to B is described with two angles, q_1 and q_2, referred to as a yaw angle and a roll angle respectively. To bring D into a general orientation with respect to B, one begins with $\hat{\mathbf{d}}_1$, $\hat{\mathbf{d}}_2$, and $\hat{\mathbf{d}}_3$ having the same directions as $\hat{\mathbf{b}}_1$, $\hat{\mathbf{b}}_2$, and $\hat{\mathbf{b}}_3$, respectively. A simple, right-handed rotation through an angle q_1 is performed about $\hat{\mathbf{b}}_3$, which is parallel to the axis of what will be called the yaw gimbal, followed by a similar rotation through an angle q_2 about $\hat{\mathbf{d}}_1$, which is parallel to the axis of what will be referred to as the roll gimbal.

Unit vector $\hat{\mathbf{d}}_3$ can be written as

$$\hat{\mathbf{d}}_3 = \sin q_1 \sin q_2 \, \hat{\mathbf{b}}_1 - \cos q_1 \sin q_2 \, \hat{\mathbf{b}}_2 + \cos q_2 \, \hat{\mathbf{b}}_3 \tag{20}$$

When $\hat{\mathbf{d}}_3$ has the same direction as $\mathbf{p}^{QP}$ [see Eq. (18)], the instrument boresight is aimed at the target point T identified in Sec. 4.2. A unit vector having the same direction as $\mathbf{p}^{QP}$ can be expressed as

$$\mathbf{r}^{QP} = \frac{\mathbf{p}^{QP}}{|\mathbf{p}^{QP}|} \triangleq r_1 \hat{\mathbf{b}}_1 + r_2 \hat{\mathbf{b}}_2 + r_3 \hat{\mathbf{b}}_3 \tag{21}$$

When the scalar measure numbers r_1, r_2, and r_3 are in hand, the angles necessary to satisfy the equation $\hat{\mathbf{d}}_3 = \mathbf{r}^{QP}$ can be determined by the relationships

$$q_1 = \arctan\left(\frac{r_1}{-r_2}\right), \qquad q_2 = \arctan\left(\frac{r_1 \sin q_1 - r_2 \cos q_1}{r_3}\right) \tag{22}$$

Thermal considerations may dictate a semi-annual change in the nominal orientation of B with respect to the local-vertical-local-horizontal reference frame of P; in particular, a

rotation of B through 180° about local vertical may be required. For a given position vector $\mathbf{r}^{QP}$, this rotation is accompanied by a change in the signs of r_1 and r_2. Equations (22) are applicable in either situation, without modification. It can be shown that the change in yaw angle does not alter q_1, whereas it changes the sign of q_2.

5 RESULTS

The material presented in Secs. 2 – 4 forms the basis of a computer program used to study intercalibration opportunities that arise under various conditions. In what follows, results are presented for a pair of spacecraft in low Earth orbits. Computations are performed at intervals of 1 second for one year of simulated orbital motion. Orbital parameters of the two spacecraft are presented in Sec. 5.1, together with a brief discussion of important consequences that follow from the particular numerical values of the parameters. The geographic and temporal distributions of opportunities are addressed in Sec. 5.2, and Sec. 5.3 contains an assessment of time during which useful measurements can be obtained. Finally, gimbal motion is quantified in Sec. 5.4. An annual perspective is provided first, followed by details of motion during two specific opportunities of interest.

5.1 Orbital Parameters

The orbital characteristics of the primary spacecraft, P, are chosen as follows. The orbit is circular (see Sec. 2.2) with an altitude of 609 km. (The value of Earth radius, R_E, is taken to be 6378 km; therefore, the radius of the orbit of P is $R_C = 6987$ km.) The inclination i of the orbit plane with respect to the equatorial plane is 90° (polar orbit); in view of Eq. (3) there is in this case no average time rate of change of the longitude of ascending node Ω and the orbit plane is fixed in an inertial reference frame. The initial value of argument of latitude u is assumed to be 0°, meaning that P is crossing the equator and headed northward at the beginning of the simulation. The value of Ω, a constant, is taken to be 0°. At the instant of autumnal equinox, $\Omega = u = 0^\circ$ corresponds to a local time of ascending node of 24:00 hours, or midnight; however, the local time of ascending node will vary during the year because this orbit is not sun-synchronous.

The secondary spacecraft A is given a circular orbit with an altitude of 833 km ($R_A = 7211$ km). The inclination i is chosen to be 98.74° in order to make the orbit sun-synchronous (see Sec. 2.3). The initial value of u is taken to be 0°, and the initial value of Ω is set to 202.5°. At the instant of autumnal equinox, these initial values correspond to a local time of ascending node of 13:30 hours, or 1 hour and 30 minutes after local noon. Orbital parameters for P and A are recorded in Table 1.

As discussed heretofore, the longitude of ascending node of the orbit of P does not change with time ($\dot{\Omega} = 0$), whereas A is in a sun-synchronous orbit ($\dot{\Omega} = n_S$). The difference in time rate of change of Ω for the two orbits leads to a change in the angle Θ between the orbit planes or, more precisely, the angle between the two orbital angular momentum vectors. A time history of Θ is shown in the upper half of Fig. 14. After 160 days the angle reaches a minimum value of 8.74°, which is the difference in inclinations of the two orbits, and a maximum of 171.26° is reached after 343 days. Θ is equal to 90°

Table 1. Orbital Parameters

Parameter	Spacecraft P		Spacecraft A 13:30 local time	
altitude (km)	(constant)	609	(constant)	833
inclination, i (deg)	(constant)	90	(constant)	98.74
longitude of ascending node, Ω (deg)	(constant)	0	$(t = 0)$	202.5
argument of latitude, u (deg)	$(t = 0)$	0	$(t = 0)$	0

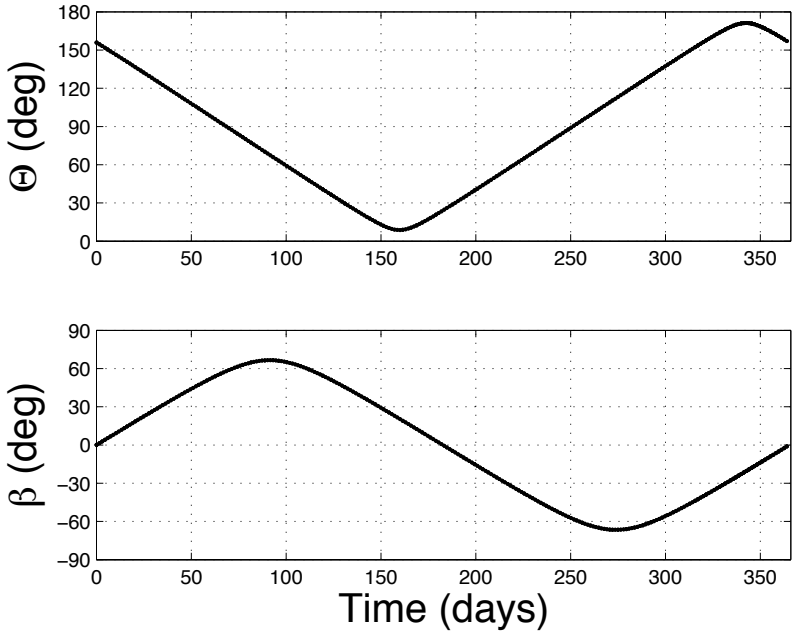

Figure 14. Angle Between Orbit Planes, Solar Beta Angle for P

on day 70 and again on day 250. When arranged in ascending order, these key days are roughly 3 months apart, and they correspond to notable features in the results that follow.

The bottom half of Fig. 14 shows a time history of the angle β between the orbit plane of P and a vector directed toward the Sun. The amplitude and phase of the curve are consequences of the particular orbital parameters for P, and the direction of the Sun at the outset of the simulation (see Sec. 2.4). Although the value of β does not affect intercalibration directly, it can affect the design and operation of the spacecraft. For example, the 180-degree rotation mentioned in Sec. 4.3 could be required when the sign of β changes, in order to keep one side of the spacecraft always shaded.

The intercalibration pyramid (see Sec. 3.3) is about 6.5 times as long as it is wide. With the aid of Eqs. (2) and (5), the angle ψ (see Fig. 6) is found to be 17.72° by using $R_A = 7211$ km and a maximum time τ between measurements of 300 sec. The value of

the angle δ, twice the scan angle of the instrument aboard A (see Sec. 3.2), is taken to be 110°. The corresponding value of ϵ (see Fig. 7) is determined to be 2.72°. Thus, $\psi/\epsilon = 6.5$.

5.2 Geographic and Temporal Distribution of Intercalibration Opportunities

The geographic distribution of intercalibration opportunities can be illustrated by plotting the ground track of P during each opportunity. Over the course of one year, 661 opportunities arise as shown in Fig. 15, where the beginning of an opportunity is indicated with an open circle, the end of an opportunity is denoted by a filled circle, and the ground track is represented by a line segment that joins two circles. Because P is traveling at a constant orbital speed, the length of a ground track is an indication of the duration of an opportunity. Opportunities with long durations occur at low to mid latitudes. Conversely, opportunities of short durations occur predominantly at high latitudes, although they can also be found at low latitudes.

Over the course of one year there is a change in the latitude at which intercalibration occurs, due to two factors. First, as the plane of the sun-synchronous orbit of A precesses, there are marked changes in the latitudes of the two points at which the ground tracks of A and P intersect. Second, the northern and southern boundaries of the terminator change in latitude during the year. These two effects combine to produce a seasonal variation in the latitude of intercalibration. For example, intercalibration takes place predominantly over northern latitudes during the first 30 days of the simulation as shown in Fig. 16. In the 30-day period that follows, almost all intercalibration occurs over extreme southern latitudes as illustrated in Fig. 17. The ground tracks contained in Fig. 18 indicate that by the middle of the year there has been a shift to low and mid latitudes. The seasonal change in intercalibration latitude is better illustrated in Fig. 19 with the temporal behavior of the latitude of P at the beginning of each opportunity. Opportunities begin at extreme latitudes when $\Theta = 90^\circ$ (see Fig. 14), whereas they begin near the equator when Θ is minimum, and maximum.

5.3 Duration of Intercalibration Opportunities

The time spent in each tent (or pyramid) over the course of a year is marked with an open triangle in Fig. 20. Seasonal behavior seen in Fig. 19 is also evident here. Two minima of about 90 sec occur six months apart, during times when intercalibration opportunities exist at near-polar latitudes (see Fig. 19) and $\Theta = 90^\circ$ (see Fig. 14). Three months after the first minimum, duration reaches a maximum of nearly 600 sec at a time when intercalibration occurs over the equator and Θ reaches a minimum; P and A are moving in roughly the same direction. Three months after the second minimum, duration reaches a local maximum of approximately 300 sec. At this time intercalibration occurs over the equator and Θ reaches a maximum, and P and A are traveling in approximately opposite directions.

No consideration is given to viewing angles (see Sec. 4.1) in the calculation of time spent in each tent, which is plotted with open triangles in Fig. 20. Now, measurements of reflected solar radiation are not useful when solar zenith angle θ_0 is greater than 75°; therefore, time spent in the tent does not always provide an accurate indication of the quantity of useful measurements that can be obtained. The effect of the constraint can be taken into

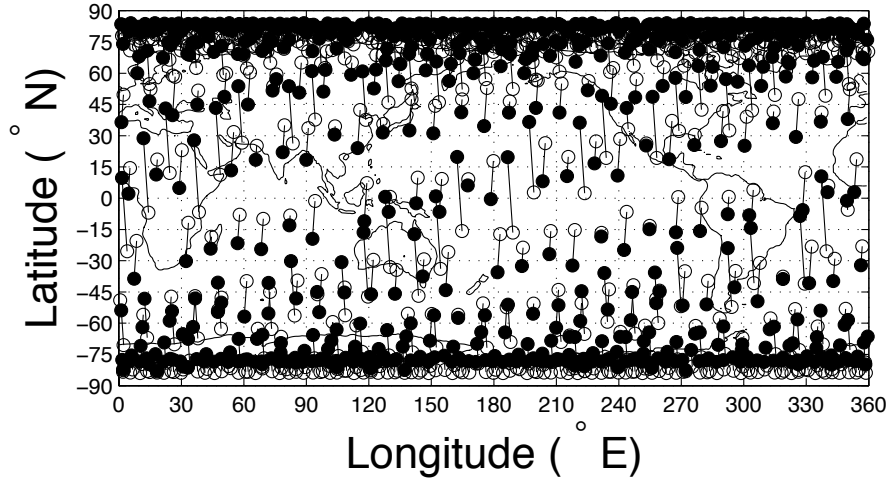

Figure 15. Ground Tracks of P During Intercalibration, One Year

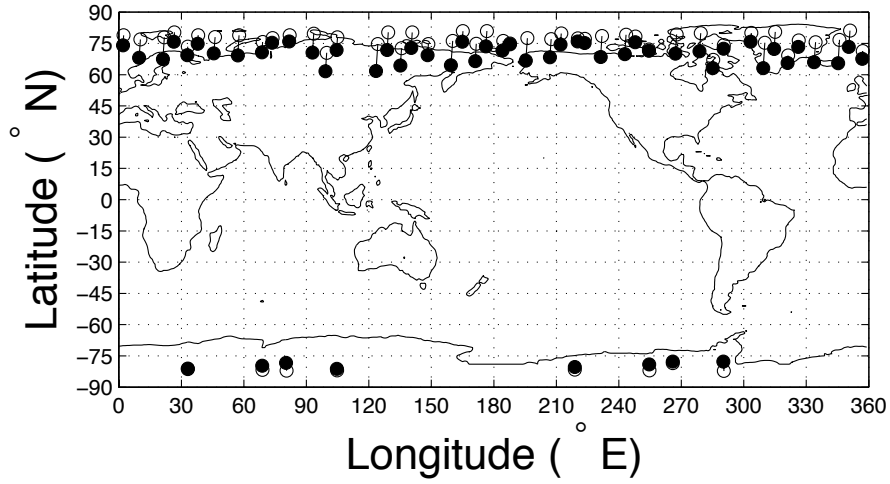

Figure 16. Ground Tracks of P During Intercalibration, Mission Days 0 – 30

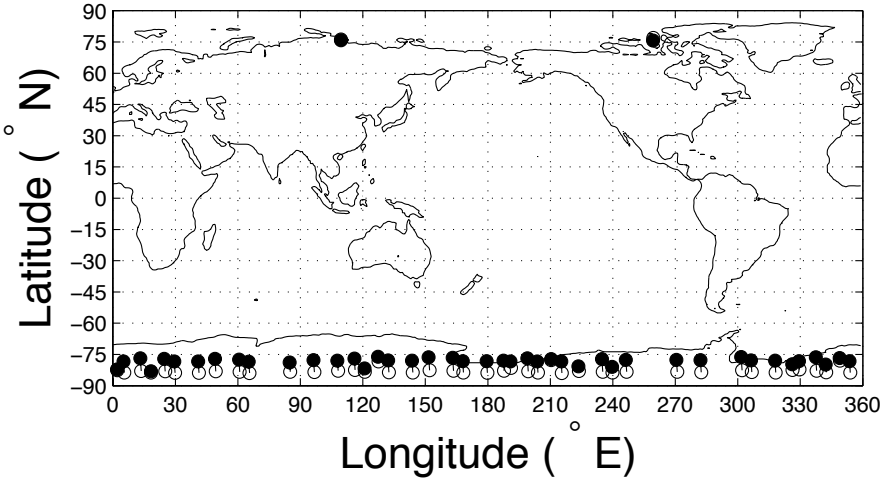

Figure 17. Ground Tracks of P During Intercalibration, Mission Days 31 – 60

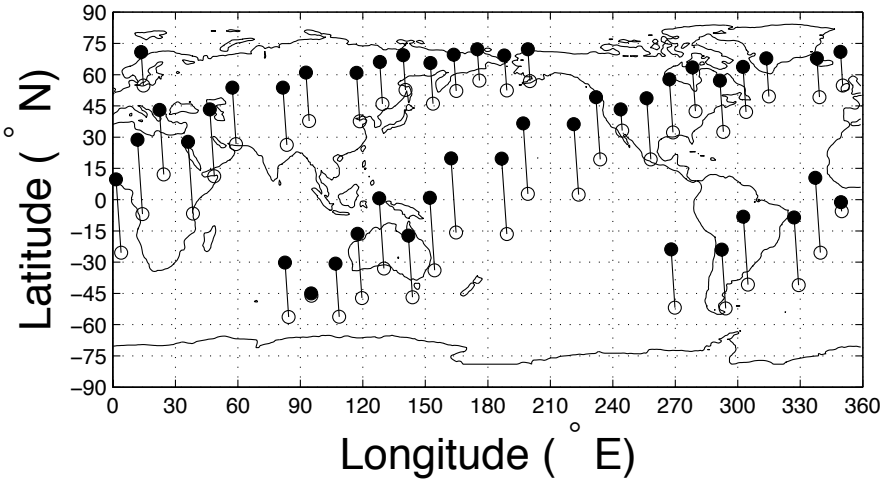

Figure 18. Ground Tracks of P During Intercalibration, Mission Days 151 – 180

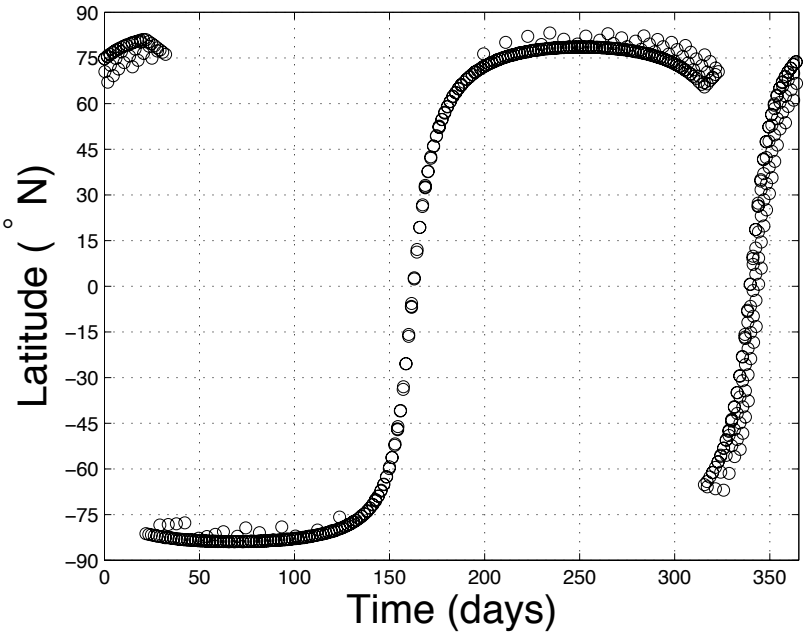

Figure 19. Latitude of P at Beginning of Intercalibration, One Year

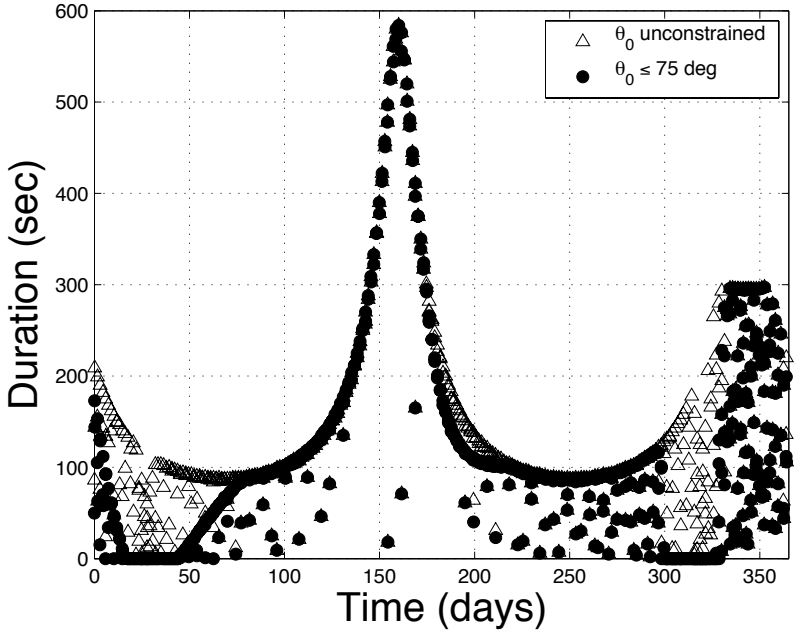

Figure 20. Duration of Intercalibration Opportunities, One Year

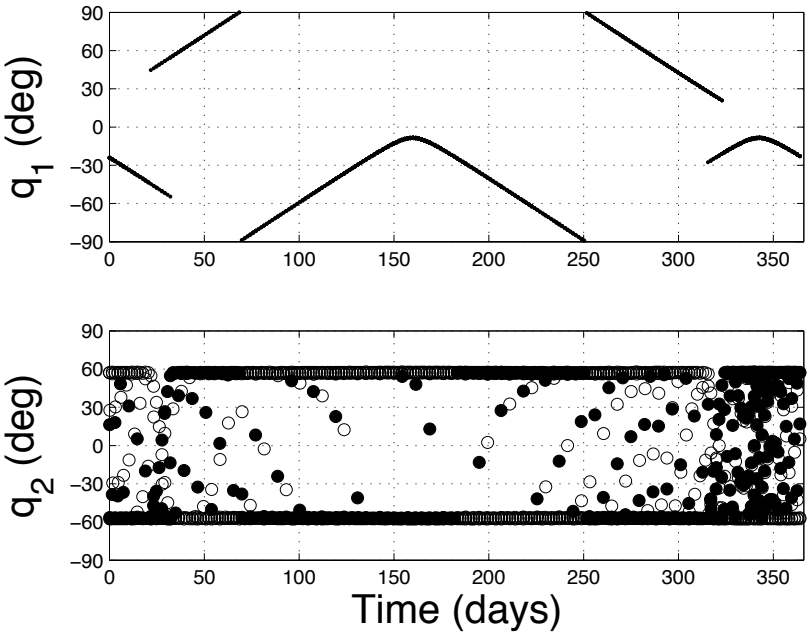

Figure 21. Gimbal Angles During Intercalibration, One Year

account by determining the time during which $\theta_0 \leq 75^\circ$ at the target of the boresight of the instrument aboard P, and the adjusted durations are shown in Fig. 20 with filled circles. It can be seen that no useful measurements can be obtained during two intervals, each lasting a substantial number of days. The first of these occurs between days 18 and 45, whereas the second period lasts from day 300 to about day 327. Duration is significantly reduced between days 0 and 18, and again between days 45 and 80.

5.4 Aiming the Boresight

The location of a target at which viewing angles for P are identical to those for A at some instant in time (within an allowable window) is discussed in Sec. 4.2. Gimbal angles q_1 and q_2 (see Fig. 13) needed to aim the boresight of the instrument aboard P at such a target are the subject of Sec. 4.3. Annual time histories of q_1 and q_2 are provided in Fig. 21.

When the spacecraft bus B (see Sec. 4.3) is in a nominal orientation with respect to the local-vertical-local-horizontal reference frame for P, unit vector $\hat{\mathbf{b}}_1$ is in the direction of the orbital (circular) velocity of P, $\hat{\mathbf{b}}_2$ has direction opposite to the orbital angular momentum vector of P, and $\hat{\mathbf{b}}_3$ is in the direction of local nadir. In this case, one can regard q_1 as an angle needed to to make unit vector $\hat{\mathbf{d}}_1$ (see Fig. 13) parallel to the ground track of A. In general there are two values of q_1 that will produce the desired result; the two values differ by 180°. Setting q_1 equal to the angle Θ between the orbit planes provides one approximate solution. By using the arctangent function as in Eq. (22) one obtains a solution that minimizes $|q_1|$, with $-90^\circ \leq q_1 \leq 90^\circ$.

An approximate limit on the magnitude of q_2 of 55° can be determined by halving the

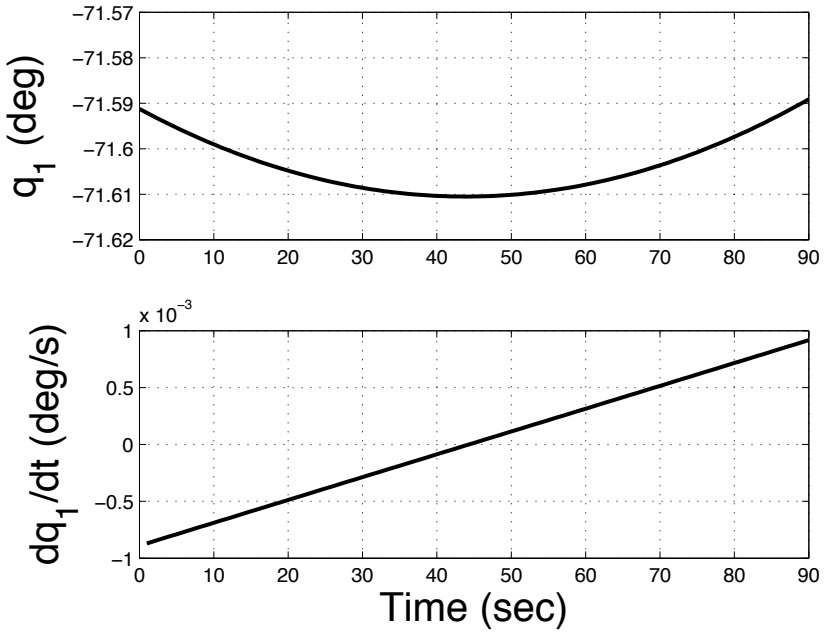

Figure 22. Yaw Gimbal Motion, Mission Day 87

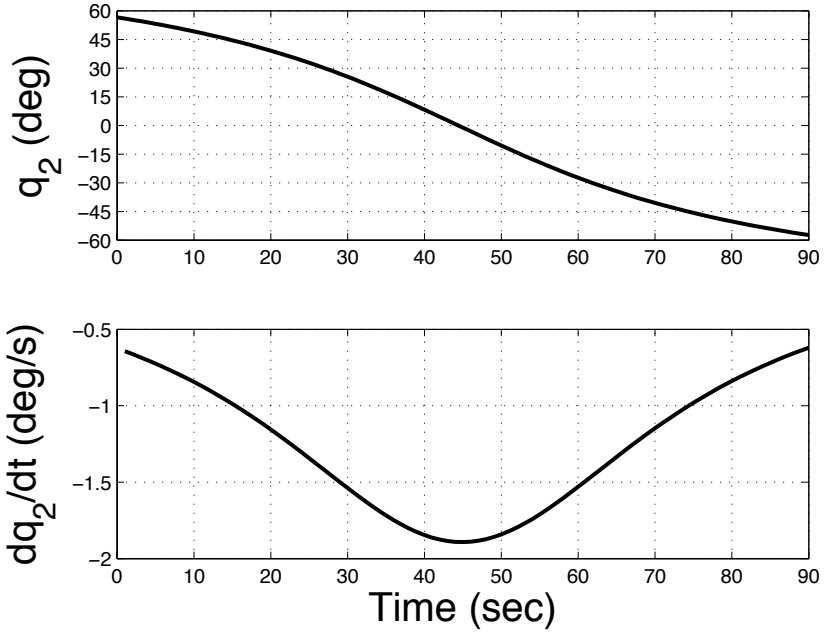

Figure 23. Roll Gimbal Motion, Mission Day 87

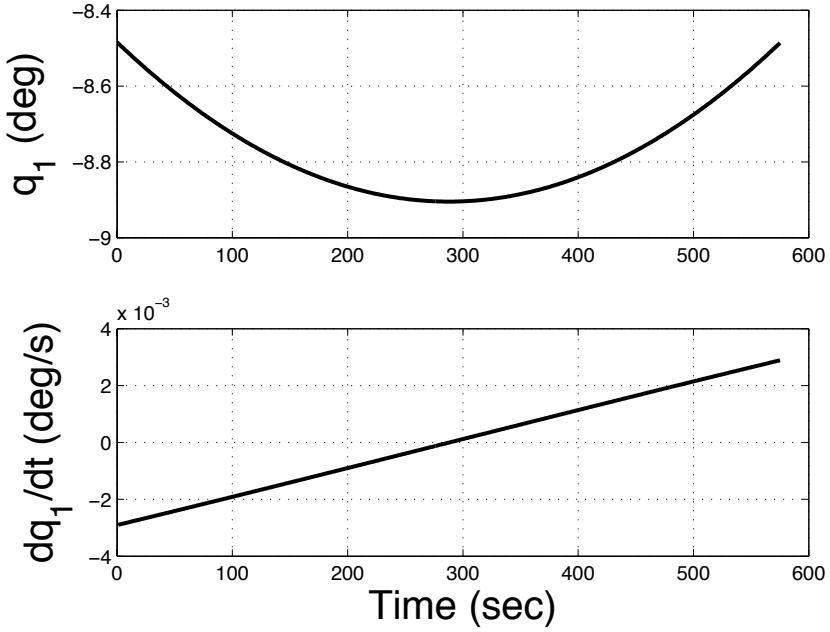

Figure 24. Yaw Gimbal Motion, Mission Day 161

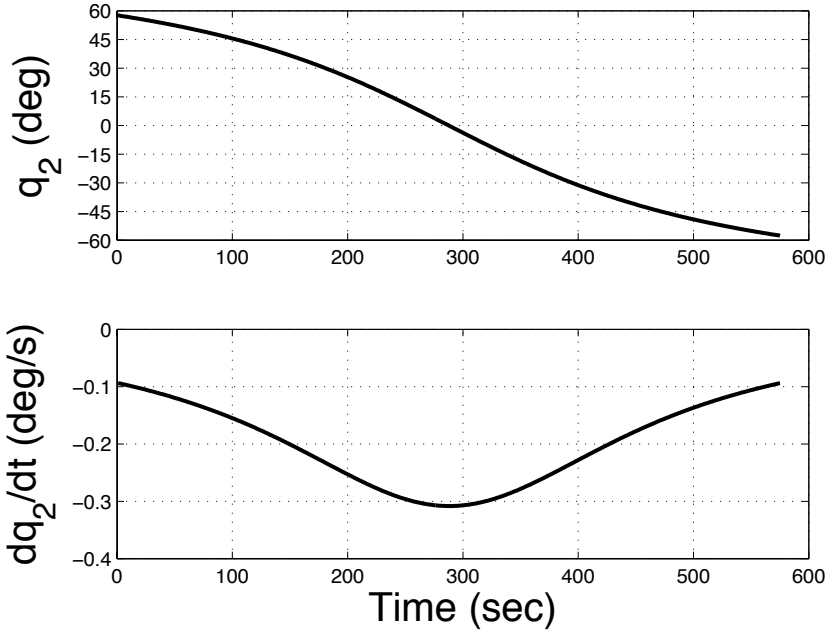

Figure 25. Roll Gimbal Motion, Mission Day 161

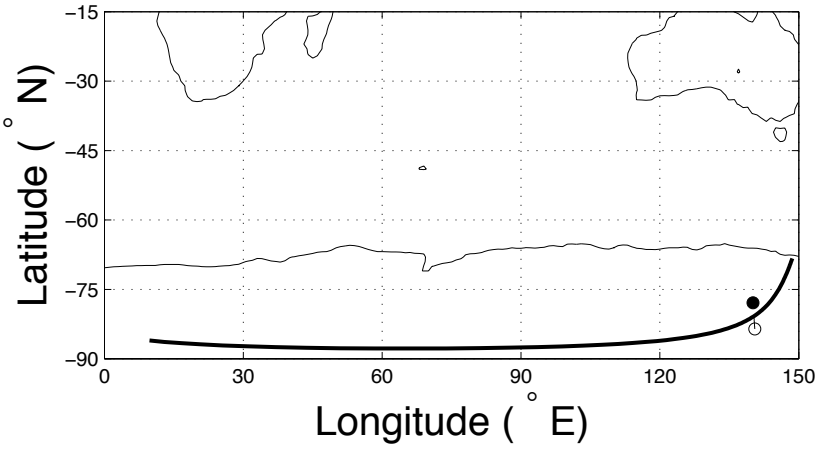

Figure 26. Boresight Track, Mission Day 87

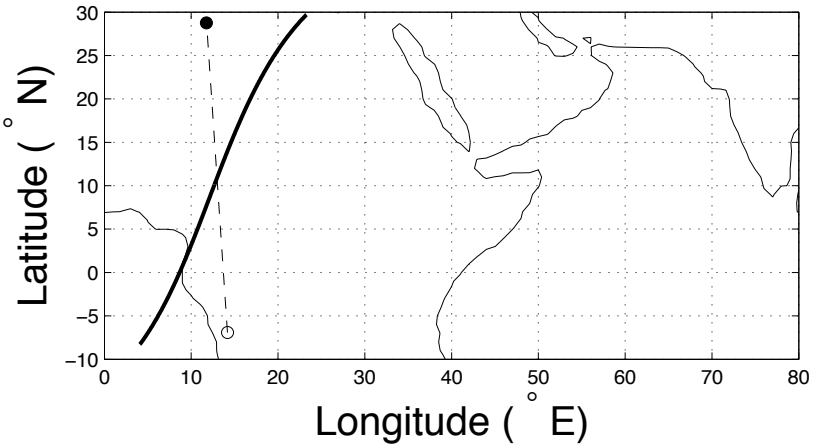

Figure 27. Boresight Track, Mission Day 161

value of δ, taken to be 110° as discussed previously. The particular values of the orbital parameters used here (see Sec. 5.1) lead to an actual limit of $|q_2| \leq 57.7^\circ$. This limit is evident in the annual time history of q_2 shown in Fig. 21, where the value at the beginning of an intercalibration opportunity is indicated with an open circle, and the value at the end of an opportunity is marked with a filled circle. When P passes through a corner of the tent (rather than all the way from one side to the other), the initial or final value of q_2 can differ substantially from 57.7°, as shown.

Details of the gimbal motion and boresight path are provided for two intercalibration opportunities of interest. The first occurs on day 87 when the duration of the opportunity is short (see Fig. 20) and intercalibration takes place over the Antarctic (see Fig. 19). The second opportunity takes place on day 161 when duration is maximum and intercalibration occurs over the equator.

Motion on day 87 is shown for the yaw gimbal in Fig. 22 and for the roll gimbal in Fig. 23. The duration of the opportunity is 90 sec. The yaw gimbal moves only slightly. Variation in q_1 is only about 0.02°, and the time-derivative of q_1 does not exceed 0.001°/sec. In contrast, there is substantial movement of the roll gimbal. The roll angle varies smoothly all the way from 57.7° at the beginning of the opportunity to -57.7° at the conclusion of the opportunity. The time-derivative of q_2 begins and ends with a value of about -0.6°/sec, and reaches -1.9°/sec when $q_2 = 0$ and the boresight is aimed at nadir. It is important to note that in other spacecraft pairings the maximum absolute value of dq_2/dt will increase as the difference in orbit radii, $R_A - R_C$, decreases.

On day 161 the variation in q_1 is approximately 0.4° as shown in Fig. 24, and the magnitude of dq_1/dt remains less than 0.003°/sec. The roll gimbal again undergoes a large excursion from 57.7° to -57.7° as seen in Fig. 25, but the 575-sec duration of the opportunity results in lower values of dq_2/dt, which range from -0.1°/sec to -0.3°/sec.

As a consequence of using the angular displacements shown in Figs. 22 and 23 to aim the boresight during the opportunity on day 87, the boresight traces a path on Earth's surface illustrated in Fig. 26 with a solid curve. Because intercalibration is taking place very near the South pole, the boresight path covers a large range of longitude during the initial portion of the opportunity. The location of the primary spacecraft at the beginning and end of the opportunity is indicated with open and filled circles, respectively, and its ground track is displayed with a dashed line. The boresight path crosses from one side of the ground track to the other when the value of q_2 is zero. At each target point on the solid curve, the three viewing angles (see Sec. 4.1) for the primary spacecraft are, by construction, identical to those for the secondary spacecraft. A similar plot of the boresight path during the opportunity on day 161 is provided in Fig. 27. In this case the boresight is aimed according to the angular displacements shown in Figs. 24 and 25. The boresight path is approximately symmetric with respect to the ground track of the primary spacecraft.

6 CONCLUSION

If accurate measurements of solar radiation reflected by Earth can be obtained from one spacecraft, they can be used to calibrate the measurements obtained by a second spacecraft. The measurements must be made within a short time of one another, and from a similar vantage point. Investigation of opportunities for intercalibration between two spacecraft

is facilitated by making several simplifying assumptions regarding orbital motion, and by introducing the geometrical concepts of an intercalibration tent, together with a pyramid. When two rotational degrees of freedom are available, the boresight of the instrument on the primary spacecraft can at each instant be aimed at a target for which there are, by construction, identical viewing angles to the primary and secondary spacecraft. Two angles, yaw and roll, are used to describe the direction of the instrument boresight relative to the primary spacecraft bus.

Key mathematical relationships presented here serve as the basis for a computer program that can be used to analyze opportunities over the course of one year (or even longer) between two spacecraft in particular orbits. Results are provided for the case of a primary spacecraft in polar orbit and the secondary spacecraft in a sun-synchronous orbit. The period of relative precession of the two orbit planes is one year; this is observed to be the period of several quantities including the angle between the two orbit planes, the latitude at which an intercalibration opportunity begins, the duration of an opportunity, and the yaw angle of the instrument boresight. Maxima and minima of these periodic variables occur at times when the angle between the orbit planes becomes 90° or reaches one of the two extrema. During a particular intercalibration opportunity there is very little variation in yaw. The roll angle, however, varies substantially. The time-derivative of roll can reach nearly 2°/sec for the orbital parameters used in the present example.

References

[1] Fox, N., et al., "Traceable Radiometry Underpinning Terrestrial- and Helio-Studies (TRUTHS)," *Advances in Space Research*, Vol. 32, No. 11, 2003, pp. 2253–2261.

[2] Fox, N. P., "TRUTHS: A benchmark mission for climate and GEOSS," *Global Space-based Inter-Calibration System Quarterly*, R. A. Iacovazzi, Jr., Editor, Vol. 4, No. 1, 2010, p. 1.

[3] Fox, N. P., "TRUTHS: SI Traceability," *Global Space-based Inter-Calibration System Quarterly*, R. A. Iacovazzi, Jr., Editor, Vol. 4, No. 1, 2010, pp. 2–3.

[4] *Earth Science and Applications from Space: National Imperatives for the Next Decade and Beyond*, National Research Council (U.S.), Committee on Earth Science and Applications from Space, National Academies Press, 2007, pp. 92–95.

[5] Anderson, D., Jucks, K. W., and Young, D. F., "The NRC Decadal Survey Climate Absolute Radiance and Refractivitiy Observatory: NASA Implementation," *International Geoscience and Remote Sensing Symposium (IGARSS)*, Vol. 3, 2008, pp. III-9–III-11.

[6] Smith, G. L., Szewczyk, Z. P., Rutan, D. A., and Lee, R. B., "Comparison of Measurements from Satellite Radiation Budget Instruments," *Journal of Geophysical Research - Atmospheres*, Vol. 111, No. D4, 2006, Article D04101.

[7] Haeffelin, M., Wielicki. B., Duvel. J. P., Priestley, K., and Viollier, M., "Intercalibration of CERES and ScaRaB Earth Radiation Budget Datasets Using Tempo-

rally and Spatially Collocated Radiance Measurements," *Geophysical Research Letters*, Vol. 28, No. 1, 2001, pp. 167–170.

[8] Szewczyk, Z. P., Smith, G. L., and Priestley, K. J., "Validation of Clouds and Earth Radiant Energy System Instruments Aboard the Terra and Aqua Satellites," *Journal of Geophysical Research - Atmospheres*, Vol. 110, No. D2, 2005, Article D02103.

[9] Battin, R. H., *An Introduction to The Mathematics and Methods of Astrodynamics*, AIAA, New York, 1987, p. 504.

[10] *The Astronomical Almanac for the Year 1999*, Nautical Almanac Office, United States Naval Observatory, U.S. Government Printing Office.

[11] Wielicki, B. A., Doelling, D. R., Young, D. F., Loeb, N. G., Garber, D. P., and MacDonnell, D. G., "Climate Quality Broadband and Narrowband Solar Reflected Radiance Calibration Between Sensors in Orbit," *International Geoscience and Remote Sensing Symposium (IGARSS)*, Vol. 1, 2008, pp. I-257–I-260.

[12] Minnis, P., Doelling, D. R., Nguyen, L., Miller, W. F., and Chakrapani, V., "Assessment of the Visible Channel Calibrations of the VIRS on TRMM and MODIS on *Aqua* and *Terra*,"*Journal of Atmospheric and Oceanic Technology*, Vol. 25, No. 3, 2008, pp. 385–400.

Reviewed by Z. Peter Szewczyk, Ph.D., Science Systems and Applications, Inc., Hampton, VA.